Multibody Syst Dyn
https://doi.org/10.1007/s11044-018-9614-y

A robust two-stage active disturbance rejection control for the stabilization of a riderless bicycle

Mauro Baquero-Suárez[1,2] · John Cortés-Romero[1] · Jaime Arcos-Legarda[1] · Horacio Coral-Enriquez[1,2]

Received: 27 June 2017 / Accepted: 5 January 2018

Abstract In this work we propose a two-stage observer-based feedback control approach to automatically stabilizing a riderless bicycle in its upright position when moving forward at a constant speed. Our strategy uses a modern control approach called Active Disturbance Rejection Control (ADRC), based on Generalized Proportional Integral (GPI) extended observers, to estimate a unified signal that groups all the discrepancies between an adopted linear model and the actual behavior of the plant. These estimations are used in the feedback controller as an additive, close cancellation and terms devising proper output feedback control laws that linearly regulate the lean angle with respect to its upright position. From a control-design perspective, the bicycle is a perturbed, uncertain system with an unstable and non-linear behavior that is strongly forward speed dependent. The ADRC scheme allows one to solve this problem easily by using a control strategy based on an acceptable mathematical model derived from lumped-parameter analysis, and its effectiveness has been validated by the successful results from real implementation experiments on an instrumented bicycle prototype. A detailed description of all the stages of the mechatronics process design is included for a proper reference.

Keywords Autonomous bicycle · Non-linear systems · Active disturbance rejection control · Generalized proportional integral control · Disturbance observers · Bicycle robot

1 Introduction

Historical studies show the scientific importance and social impact that bicycles have had through time. Since the first invention by von Drais in 1817, followed by the velocipede invented by Michaux in 1861, the Penny Farthing model by Humber in 1882 and other

✉ J. Cortés-Romero
jacortesr@unal.edu.co

1 Department of Electrical Engineering, National University of Colombia, Av. K30 No. 45-03, Edif. 411 Of. 203A, Bogotá D.C., Colombia

2 Engineering Faculty, University of San Buenaventura, Av. K8H No. 172-20, Edif. Diego Barroso Of. 204, Bogotá D.C., Colombia

Published online: 25 January 2018

bicycle prototypes throughout the history that have made possible the recent bicycles in modern times [1–3]. A bicycle is statically unstable, but under certain forward speed range, it can automatically steer itself and recover from the fall due to gyroscopic precession of the front wheel. However, the possibility of the bicycle self-stability without this effect was reported in [4]. This interesting behavior has attracted the attention of many researchers, for instance, in [5–8] an important review about dynamic analysis of single-track vehicles (bicycles and motorcycles) from a control perspective was reported. On the other hand, the bicycle is a non-linear system, strongly forward speed dependent, whose complex dynamics and external disturbances are difficult to completely model given its unstable nature. This system can exhibit non-minimal phase zeros at low forward speed range. For this reason, a satisfactory control strategy must be sufficiently robust to achieve a bicycle stabilization that maintains its upright position while rejecting all the external disturbances that affect the system despite the uncertain model used for the design. The stabilization of bicycles is a serious topic in the field of control systems, whose understanding could serve for: (1) The stabilization of more complex unstable systems; (2) The building of adapted bicycles for teaching children with disabilities (see [9, 10]); and (3) the development of single-track mobile robots more efficient than double-track ones, among other applications.

A comprehensive review of available methods for the control of bicycle stabilization is definitely beyond the scope of this paper. However, some works deserved our attention. The state-feedback controllers tuned by the Linear–Quadratic Regulator (LQR) method in [11–13], the Model Predictive Control (MPC) scheme in [14] and the Fault Tolerant Control (FTC) techniques in [15–17], use optimization methods that require bicycle detailed models. The strategies under Feedback Linearization (FL) approach proposed in [18–20], were based on extensive non-linear models obtained by Lagrange method, which led to the design of complex non-linear controllers. The effectiveness of the previously mentioned strategies were only validated by simulations with some selected complex bicycle models, and none of them presented a real implementation.

Other contributions show successful results of their stability control proposal implemented on a real bicycle. Both the PD control strategy in [21] and the Sliding Mode Control (SMC) in [22] use disturbance observers for improving the performance and robustness of stabilization, even though they were implemented on an instrumented bicycle placed on a fixed platform, which achieves a suitable environment that minimizes the external disturbance effects, similar to the experiments made with the Adaptive Neuro-Fuzzy control proposed in [23]. It would be really interesting to prove and compare these strategies on a free moving standard bicycle. The Linear Parameter Varying (LPV) state-feedback controller proposed in [24] has self-adjusting gains by solving a set of Linear Matrix Inequalities (LMIs) as a function of the forward speed that stabilized the bicycle in a range of 2.1 to 1 m/s during 10 s. Unlike previous references, the current work presents experimental results considering unadapted runways to further test robust control strategies.

In this paper, the problem of stabilization of a moving riderless bicycle at constant forward speed is addressed through the ADRC methodology. ADRC is a developed technique designed to control linear and non-linear uncertain systems providing robust reference tracking with improved disturbance rejection properties. The philosophy of active disturbance rejection has its theoretical foundations in [25–27] and it has been mainly led by Han and Gao. Presently, an interesting book [28] has been recently published by Sira-Ramírez which formulates the ADRC methodology through a flatness-based approach. Under that approach, Sira-Ramírez has also directed some closely related techniques called GPI observer-based Control and robust GPI Control (see [29–31]). Currently, ADRC has been extended and applied to several fields; see for example in citations [32–37].

In the proposed scheme, the unmodeled dynamics related to endogenous state-dependent non-linearities, parameter uncertainty associated to a bicycle model and external disturbances, all affecting the lean angle dynamics, are lumped into an unknown time function that is estimated by means of a GPI observer and rejected in real-time through a linear state-feedback control law that introduces this estimation [38, 39]. The GPI observation scheme is able to simultaneously estimate the referred unified disturbance input and the unmeasured states required for the state feedback. The closed-loop system under the GPI observer-based control strategy recovers the performance of the nominal linear model as long as the observer gains become sufficiently high, allowing a simple linear control law to ensure regulation of the reference tracking error to zero and making possible a robust stabilization of the bicycle in its upright position.

The strategy is designed on the basis of a perturbed linear model, so the extracted linear behavior is represented by a transfer function which, in this case, exhibits minimum phase zeros. In general, the technique is robust to the parameter variation without compromising trajectory tracking. In particular, this proposal has suitable structural controller adaptations that allow for a large variation of the parameters of the numerator and therefore of the zeros of the equivalent transfer function. The proposed controller casts into the, so-called, two-stage (inner loop–outer loop) controller design. In the first stage, the steering angle $\delta(t)$ is taken as an auxiliary control input acting in an outer-loop lean angle controller. In the second stage, the designed steering angle is taken as our reference signal to be tracked on the basis of the armature voltages, acting as an inner-loop controller. Although the control proposal is based on lumped-parameter models, its effectiveness is validated by both multibody MATLAB co-simulation and a real implementation on an instrumented bicycle prototype.

The rest of this paper is organized as follows. Section 2 shows the modeling of the robot bicycle. Section 3 presents the proposed control strategy. Section 4 describes the prototype construction and explains the controller implementation. Section 5 gives the obtained results in the experiments. Finally, some conclusions are outlined in Sect. 6.

2 Modeling of the riderless bicycle

The purpose of the model used in this paper is to develop a control system to stabilize the lean angle dynamics with respect to the upright position. Moreover, the developed model will allow the balancing problem of a riderless bicycle to be analyzed and to define the restrictions on the bicycle's operating conditions. The mathematical model developed by Whipple in 1899 [40] is used to describe the dynamic behavior of the riderless bicycle. This model is based on the analysis of the multibody dynamics of the prototype shown in Fig. 1(a) and its detailed CAD version shown in Fig. 1(b). In order to get a multibody model, the bicycle was divided into four rigid bodies. The first body is the rear wheel **R** shown in Fig. 1(c), which is coupled to an electric motor to move the whole system forwards. The second one is the main frame of the bicycle denoted by **T** in Fig. 1(d), which has the batteries, actuators, sensors and circuitry attached. The third one is the structure formed by the handlebar and fork, called the front frame and denoted by **H** in Fig. 1(e). It is driven by a second electric actuator in charge of the control of the bicycle's direction. The last one is the front wheel **F** presented in Fig. 1(f), which is attached to the fork by a hinge joint.

The four bodies are interconnected by revolute joints and all of them are symmetric with respect to the plane xz (see Fig. 2). The interaction between the non-slipping wheels and the flat level terrain is modeled by holonomic constraints in the normal direction and by non-holonomic constraints in the longitudinal and lateral directions. These assumptions

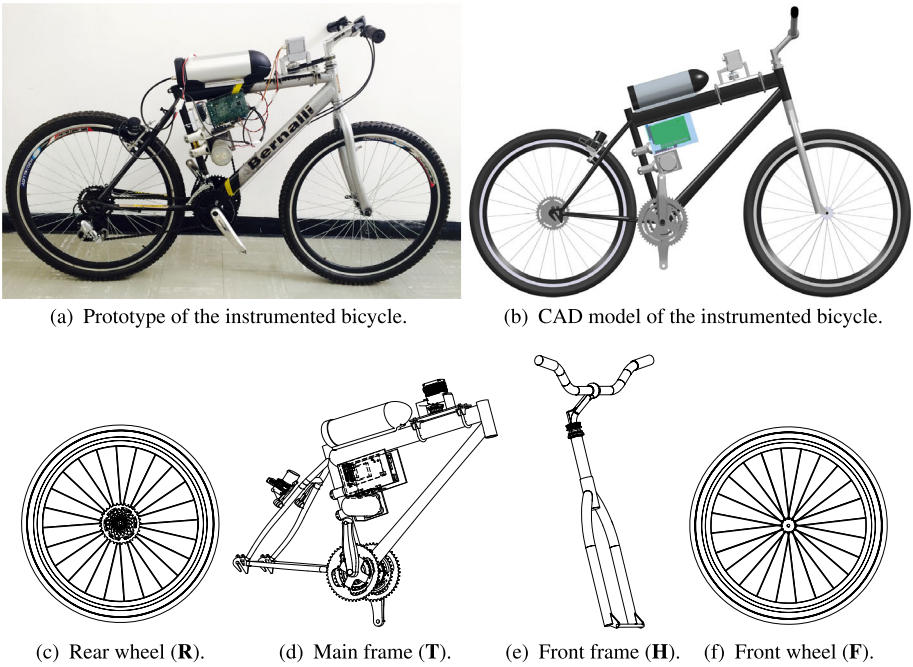

(a) Prototype of the instrumented bicycle. (b) CAD model of the instrumented bicycle.

(c) Rear wheel (**R**). (d) Main frame (**T**). (e) Front frame (**H**). (f) Front wheel (**F**).

Fig. 1 Robot bicycle prototype and its respective CAD model divided into four parts

Fig. 2 Conceptual scheme of a basic bicycle

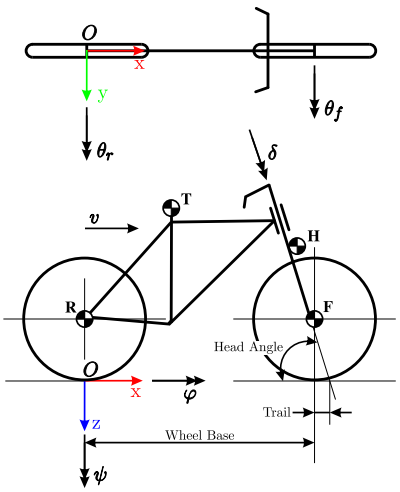

make this conceptual system energy-conserving. The global cartesian coordinate system is located at the rear wheel contact point O, with positive x pointing towards the front contact point, positive z pointing down and the positive y pointing to the bicycle's right. Figure 2 shows the conceptual bicycle scheme with its four rigid bodies characterized by lumped parameters, its coordinates system (x, y, z) and its three degrees of freedom, which are, the lean angle $\varphi(t)$, the steering angle $\delta(t)$ and the forward speed defined as $v(t)$.

Table 1 Basic bicycle parameters

Assembly parameters		
Parameter	Symbol	Value
Bicycle total mass	m_t	19.396 kg
Wheel base	w	1.060 m
Height of whole bicycle center of mass	h	0.563 m
Horizontal distance from (x, y, z) to whole bicycle center of mass	b	0.495 m
Trail	t_r	0.062 m
Head angle	η	74.099°
Gravity	g	9.807 m/s^2

Bodies parameters				
Parameter	Rear wheel	Main frame	Front frame	Front wheel
Mass [kg]	2.608	12.787	1.950	2.051
Inertia tensor				
J_{xx} [kg m^2]	0.090	0.559	0.144	0.089
J_{yy} [kg m^2]	0.177	0.907	0.126	0.177
J_{zz} [kg m^2]	0.090	0.384	0.025	0.089
J_{xz} [kg m^2]	0.000	0.135	−0.015	0.000
Center of mass $(\bar{x}, \bar{z})$ [m]	(0, −0.324)	(0.438, −0.621)	(0.943, −0.753)	(1.060, −0.324)

A simplified linear model presented by Papadopoulos in [8, 41] is regarded as base model. It is composed of two dynamically coupled second order differential equations, which are shown in a compact form here:

$$\mathbf{M}\ddot{\mathbf{q}}(t) + v(t)\mathbf{C}_1\dot{\mathbf{q}}(t) + \left(g\mathbf{K}_0 + v(t)^2\mathbf{K}_2\right)\mathbf{q}(t) = \mathbf{f}(t), \tag{1}$$

where

$$\mathbf{q}(t) = \begin{bmatrix} \varphi(t) & \delta(t) \end{bmatrix}^{\mathrm{T}} \quad \text{and} \quad \mathbf{f}(t) = \begin{bmatrix} T_\varphi(t) & T_\delta(t) \end{bmatrix}^{\mathrm{T}}.$$

$T_\varphi(t)$ is the lean torque considered as exogenous disturbance, $T_\delta(t)$ is the steering torque applied to handlebar axis. $\mathbf{M}$ is a symmetric and invertible matrix which represents the mass and inertia properties. The damping effects are included in $v(t)\mathbf{C}_1$, they depend on forward speed and capture gyroscopic torques from rear wheel's acceleration, steer and lean rates. Finally, the stiffness and gravitational terms, $g\mathbf{K}_0 + v(t)^2\mathbf{K}_2$, depend on the forward velocity, gravity acceleration, gyroscopic and centrifugal effects. Note that the model described by (1) is obtained from a linearization around the equilibrium point $[\delta = 0, \varphi = 0]$ under the assumption that the bicycle is moving with constant forward speed v. Therefore, the equations that describe the bicycle's model are only valid under small perturbations of those variables around the equilibrium point. Hence, under varying forward speed, the model is an approximation and becomes more precise as the acceleration gets smaller.

2.1 Parameters characterization

The bicycle's physical parameters are consigned in Table 1, which were obtained from direct measure on the prototype and the CAD bicycle's model. As presented in [8], the bicycle's

parameters were used to compute matrices $\mathbf{M}$, $\mathbf{C}_1$, $\mathbf{K}_0$ and $\mathbf{K}_2$. Their results are presented here:

$$\mathbf{M} = \begin{bmatrix} 7.427 & 0.438 \\ 0.438 & 0.167 \end{bmatrix}, \qquad \mathbf{C}_1 = \begin{bmatrix} 0 & 6.362 \\ -0.585 & 0.607 \end{bmatrix},$$
$$\mathbf{K}_0 = \begin{bmatrix} -10.941 & -0.665 \\ -0.665 & -0.182 \end{bmatrix}, \qquad \mathbf{K}_2 = \begin{bmatrix} 0 & 10.915 \\ 0 & 0.739 \end{bmatrix}. \tag{2}$$

The differential equation (1) is written in its state space form as below:

$$\begin{aligned} \dot{\mathbf{x}}_m(t) &= \mathbf{A}(v)\mathbf{x}_m(t) + \mathbf{B}u_m(t) + \mathbf{B}_1\xi(t), \\ \mathbf{y}_m(t) &= \mathbf{C}\mathbf{x}_m(t) + \mathbf{D}u_m(t), \end{aligned} \tag{3}$$

where $\mathbf{x}_m(t) = [\varphi(t)\ \ \delta(t)\ \ \dot{\varphi}(t)\ \ \dot{\delta}(t)]^{\mathrm{T}}$ is the state vector, $u_m(t) = T_\delta(t)$ is the control system input, $\xi(t) = T_\varphi(t)$ acts as external disturbance and $\mathbf{y}_m(t) = [\varphi(t)\ \ \delta(t)]^{\mathrm{T}}$ is the output vector. Matrices $\mathbf{A}(v)$, $\mathbf{B}$, $\mathbf{C}$ and $\mathbf{D}$ are described by

$$\mathbf{A}(v) = \begin{bmatrix} \mathbf{0} & \mathbf{I} \\ -\mathbf{M}^{-1}(g\mathbf{K}_0 + v(t)^2\mathbf{K}_2) & -\mathbf{M}^{-1}(v(t)\mathbf{C}_1) \end{bmatrix},$$
$$\mathbf{B} = \begin{bmatrix} \mathbf{0} \\ \mathbf{M}^{-1}\begin{bmatrix} 0 \\ 1 \end{bmatrix} \end{bmatrix}, \qquad \mathbf{B}_1 = \begin{bmatrix} \mathbf{0} \\ \mathbf{M}^{-1}\begin{bmatrix} 1 \\ 0 \end{bmatrix} \end{bmatrix}, \qquad \mathbf{C} = \begin{bmatrix} 1 & 0 & 0 & 0 \\ 0 & 1 & 0 & 0 \end{bmatrix}, \qquad \mathbf{D} = \begin{bmatrix} 0 \\ 0 \end{bmatrix}.$$

The dependence of $\mathbf{A}(v)$ on the forward speed $v(t)$, qualifies the bicycle as a LPV system. The eigenvalues and zeros of the model (1) were computed for an interval of $v(t) = [0, 10]$ m/s, their real parts were plotted as a function of $v(t)$ in Figs. 3(a) and 3(b), respectively. Primarily, from the evolution of the real part of the eigenvalues, it is possible to see a range of forward speed between 3.15 m/s and 3.95 m/s for which all of the system's eigenvalues become negative and transform the system into a self-stable one. On the other hand, the evolution of the real part of the zeros shows that for velocities below 0.78 m/s the system becomes non-minimum phase, which implies an unstable zero dynamics. Therefore, the control strategy developed in this paper is restricted to the minimum-phase operation of the system, thus, the operation velocity considered is higher than 0.78 m/s.

2.2 Virtual dynamic model built in ADAMS™ software

Taking advantage of the detailed CAD model developed for the instrumented bicycle, a virtual dynamic model was built with the objective of simulating the more relevant dynamics of the prototype when in motion. This renders a more realistic way than performing the validation with the mathematical model. This virtual model was made in the ADAMS/View environment of multibody dynamics simulation software, MSC ADAMS, which it is characterized as Fig. 4 shows. Here, the input variables (steering torque, rear wheel torque, and disturbances on rear frame and handlebar) are manipulated, and the output variables (lean angle, steering angle, angular speed of rear wheel and simulation time) are measured.

The CAD model was exported to ADAMS/View with its mechanical properties, and all its elements were grouped into the four bodies that Fig. 1 shows. Then the virtual model's four rigid bodies were interconnected by revolute joints, which were configured

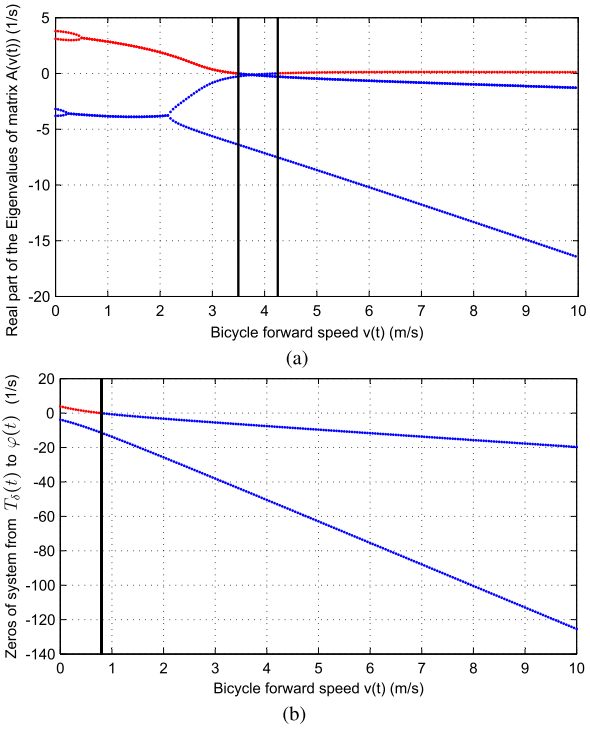

Fig. 3 (**a**) Real part of the Eigenvalues of matrix $A(v(t))$ as a function of the speed $v(t)$. (**b**) Real part of the zeros of (3) from $T_\delta(t)$ to $\varphi(t)$ as a function of speed $v(t)$

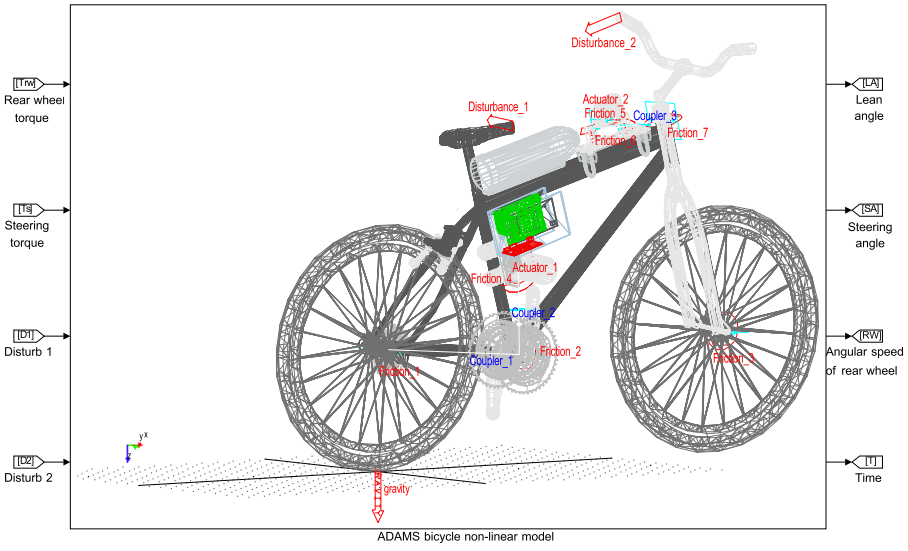

Fig. 4 Virtual dynamic model of the prototype

to be motion-resistant by the velocity-based friction model described in [42]. This friction model is available in Adams/Solver code to simulate the frictional torque dynamics generated along the rotation axis of any revolute joint as Fig. 5(a) shows.

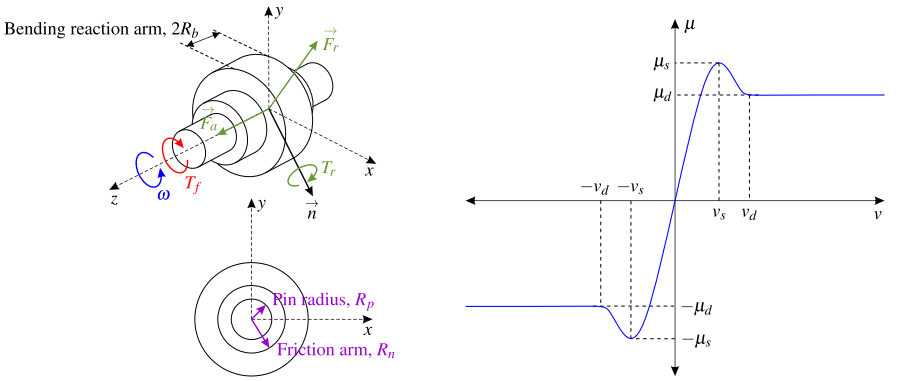

(a) Free body diagram of revolute joints.

(b) Behavior of the friction coefficient in function of the joint linear velocity.

Fig. 5 Frictional torque dynamics for the joints

Table 2 Parameters to model frictional torque in the bicycle joints

Parameters for the bicycle joints		
Static friction coefficient	μ_s	0.05
Dynamic friction coefficient	μ_d	0.03
Friction arm	R_n	0.15 m
Pin radius	R_p	0.10 m
Bending reaction arm	R_b	0.10 m
Stiction transition velocity	v_s	0.10 m/s
Dynamic transition velocity	v_d	$1.5v_s$
Friction torque preload	T_{pre}	0.05 N m
Switched effects in Adams		
Reaction force	On	
Preload	On	
Bending moment	On	

F_a and F_r are the joint reaction forces. T_r is the bending moment. R_p, R_n and R_b are the corresponding pin radius, friction arm and bending reaction arm. T_f is the resulting friction torque from the following expression:

$$T_f(t) = \mu\left[R_n\left|F_a(t)\right| + R_p\sqrt{F_{r_x}(t)^2 + F_{r_y}(t)^2} + \frac{R_p}{R_b}T_r(t) + T_{\text{pre}}\right], \tag{4}$$

assuming also the addition of a preload torque T_{pre}. μ depicts the friction coefficient, whose value varies depending on three friction regimes (static friction, dynamic friction and a transition state between both) in function of the joint linear velocity magnitude as Fig. 5(b) shows. This kind of revolute joint was assumed for all bodies of the virtual model (see Fig. 5(a)), and all of them were configured by the consigned parameters in Table 2. Linear velocities transitions v_s and v_d are related to the joint angular velocity as $v_s = R_p\omega_s$ and $v_d = R_p\omega_d$, where then ω_s and ω_d are the angular velocity transitions.

Table 3 Parameters to model friction and contact forces between the road and the bicycle's tires

Impact normal force	
Parameters	Material
	Rubber vs. asphalt
Stiffness	1×10^8 N/m
Damping	1×10^4 N s/m
Penetration depth	1×10^{-4} m
Force exponent	2.2
Coulomb friction force	
Parameters	Material
	Rubber vs. asphalt
Static coefficient [μ_{sr}]	0.72
Dynamic coefficient [μ_{dr}]	0.72
Stiction transition velocity [v_s]	0.2 m/s
Friction transition velocity [v_d]	1.0 m/s

In this virtual model, a flat and solid road was created also by CAD software for moving the bicycle on it. The contact forces between this road and the bicycle's wheels were modeled by using the established constraints in Table 3.

Finally, a similar co-simulation as in [43] was developed, where the proposed control system implemented in MATLAB/Simulink was linked with this virtual dynamic model to manipulate its actuators and govern its outputs according to the control proposal.

3 Control strategy formulation

This section describes in detail the proposed control scheme to automatically stabilize a riderless bicycle around its upright position assuming constant/slow-rate forward speed. On one hand, the forward speed of the bicycle, $v(t)$, is regulated to a desired nominal speed, $v^*(t)$, through a PI controller designed to command the traction system of the bicycle. On the other hand, the lean angle of the bicycle, $\varphi(t)$, is controlled by a two-stage active disturbance rejection control strategy, made-up of both a stabilizing controller and a tracking controller that constitute the main contribution of this work. In the first stage, an outer controller (the stabilizing controller) based on the lean angle, generates the desired angular position $\delta^*(t)$ required in the steering system to stabilize the bicycle. Then, in the second stage, an inner control loop (the tracking controller) forces the steering angle $\delta(t)$ of the bicycle to track this desired angle by applying the required torque $T_\delta(t)$ in the steering system. Figure 6 shows the block diagram of the proposed two-stage control structure for stabilizing the bicycle, and the control loop to ensure a constant/slow-rate forward speed of the bicycle.

3.1 Lean angle control loop

The bicycle model (3) can alternatively be described by

$$\ddot{\mathbf{q}}(t) + \bar{\mathbf{C}}\dot{\mathbf{q}}(t) + \bar{\mathbf{K}}\mathbf{q}(t) = \bar{\mathbf{M}}\mathbf{f}(t), \tag{5}$$

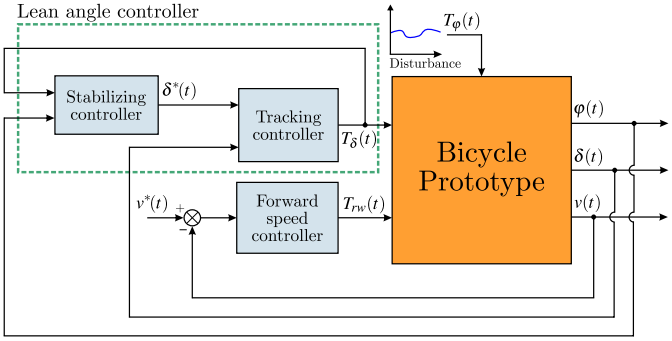

Fig. 6 General control scheme for the stabilization of the bicycle

where

$$\bar{\mathbf{C}} = v(t)\mathbf{M}^{-1}\mathbf{C_1} = \begin{bmatrix} \bar{c}_{11} & \bar{c}_{12} \\ \bar{c}_{21} & \bar{c}_{22} \end{bmatrix}, \tag{6}$$

$$\bar{\mathbf{K}} = \mathbf{M}^{-1}\left(g\mathbf{K_0} + v(t)^2\mathbf{K_2}\right) = \begin{bmatrix} \bar{k}_{11} & \bar{k}_{12} \\ \bar{k}_{21} & \bar{k}_{22} \end{bmatrix}, \tag{7}$$

$$\bar{\mathbf{M}} = \mathbf{M}^{-1} = \begin{bmatrix} \bar{m}_{11} & \bar{m}_{12} \\ \bar{m}_{21} & \bar{m}_{22} \end{bmatrix}. \tag{8}$$

Then the system dynamics takes the following form:

$$\ddot{\varphi}(t) + \bar{c}_{11}\dot{\varphi}(t) + \bar{c}_{12}\dot{\delta}(t) + \bar{k}_{11}\varphi(t) + \bar{k}_{12}\delta(t) = \bar{m}_{11}T_\varphi(t) + \bar{m}_{12}T_\delta(t), \tag{9}$$

$$\ddot{\delta}(t) + \bar{c}_{21}\dot{\varphi}(t) + \bar{c}_{22}\dot{\delta}(t) + \bar{k}_{21}\varphi(t) + \bar{k}_{22}\delta(t) = \bar{m}_{21}T_\varphi(t) + \bar{m}_{22}T_\delta(t), \tag{10}$$

which will be used to propose the outer and the inner control loops.

3.1.1 Outer control loop: stabilizing controller

According to the bicycle's model (9), the lean angle dynamics is described by

$$\ddot{\varphi}(t) = -\left(\bar{c}_{12}\dot{\delta}(t) + \bar{k}_{12}\delta(t)\right) + \bar{m}_{11}T_\varphi(t) + \bar{m}_{12}T_\delta(t) - \bar{c}_{11}\dot{\varphi}(t) - \bar{k}_{11}\varphi(t), \tag{11}$$

which contains a zero dynamics (from δ to φ) according to the transfer function given by $\frac{\varphi(s)}{\delta(s)} = \frac{-(\bar{c}_{12}s+\bar{k}_{12})}{s^2+\bar{c}_{11}s+\bar{k}_{11}}$. This zero could be minimum or non-minimum phase, depending on the bicycle's forward speed (see Fig. 3(b)). Then, lumping together some terms, a simplified version for the lean angle dynamics is found:

$$\ddot{\varphi}(t) = u_\varphi(t) - \bar{c}_{11}\dot{\varphi}(t) - \bar{k}_{11}\varphi(t) + \bar{m}_{12}T_\delta(t) + \xi_\varphi(t), \tag{12}$$

with

$$u_\varphi(t) = -\left(\bar{c}_{12}\dot{\delta}(t) + \bar{k}_{12}\delta(t)\right), \tag{13}$$

$$\xi_\varphi(t) = \bar{m}_{11}T_\varphi(t), \tag{14}$$

where $u_\varphi(t)$ is an auxiliary control input and $\xi_\varphi(t)$ is a disturbance signal which is intended to be estimated and rejected by the proposed control scheme. Note that coefficients $\bar{c}_{12}$ and $\bar{k}_{12}$ in (13) have the same sign as long as the bicycle's forward speed is greater than 0.78 m/s, which ensures a minimum-phase zero.

Remark 1 Note that nominal system (11) is represented as a simplified version (12), according to the following description:

$$\ddot{\varphi}(t) = \underbrace{\left(-\bar{c}_{12}\dot{\delta}(t) - \bar{k}_{12}\delta(t)\right)}_{u_\varphi(t)} - \bar{c}_{11}\dot{\varphi}(t) - \bar{k}_{11}\varphi(t) + \bar{m}_{12}T_\delta(t) + \underbrace{\bar{m}_{11}T_\varphi(t)}_{\xi_\varphi(t)},$$

where the disturbance signal $\xi_\varphi(t)$ contains the external term $\bar{m}_{11}T_\varphi(t)$. However, without the loss of generality, the system can also be reformulated taking into account parametric uncertainties that explicitly depend on the bicycle's forward speed, e.g. $\{\bar{k}_{12}, \bar{c}_{12}\}$:

$$\begin{aligned}\ddot{\varphi}(t) = &\left(-\bar{c}_{12}\dot{\delta}(t) - \bar{k}_{12}\delta(t) + \Delta\bar{k}_{12}\delta(t) + \Delta\bar{c}_{12}\dot{\delta}(t)\right)\\ &- \bar{c}_{11}\dot{\varphi}(t) - \bar{k}_{11}\varphi(t) + \bar{m}_{12}T_\delta(t) + \bar{m}_{11}T_\varphi(t).\end{aligned}$$

Thus, each actual parameter is composed of its nominal value (e.g. $\bar{k}_{12}$) in addition to a perturbation (e.g. $\Delta\bar{k}_{12}$) which can be time-varying. Therefore, the system results in

$$\begin{aligned}\ddot{\varphi}(t) = &\underbrace{\left(-\bar{c}_{12}\dot{\delta}(t) - \bar{k}_{12}\delta(t)\right)}_{u_\varphi(t)} - \bar{c}_{11}\dot{\varphi}(t) - \bar{k}_{11}\varphi(t) + \bar{m}_{12}T_\delta(t)\\ &+ \underbrace{\bar{m}_{11}T_\varphi(t) + \Delta\bar{k}_{12}\delta(t) + \Delta\bar{c}_{12}\dot{\delta}(t)}_{\xi_\varphi(t)},\end{aligned}$$

where $\xi_\varphi(t)$ now contains, in a unified way, external disturbances and endogenous perturbations mainly caused by uncertainty on system parameters sensitive to bicycle's forward speed variations.

In order to provide estimations of both the states and the disturbance signal of system (12), a state space description of (12) is obtained and a disturbance model approximation is assigned into the disturbance signal $\xi_\varphi(t)$. In this case, due to the relatively slow-rate variations of the bicycle lean angle, a first order linear approximation is used as the internal model of $\xi_\varphi(t)$, that is,

$$\dot{\xi}_\varphi(t) \approx 0. \tag{15}$$

Thus, an augmented system representation is found, where the states of system (12) and the states of the disturbance model approximation (15), are part of the model:

$$\dot{\mathbf{x}}(t) = \mathbf{A_o}\mathbf{x}(t) + \mathbf{B_o}u_\varphi(t) + \mathbf{E_o}T_\delta(t) + \mathbf{F_o}\dot{\xi}_\varphi(t), \tag{16}$$

$$\varphi(t) = \mathbf{C_o}\mathbf{x}(t), \tag{17}$$

with

$$\mathbf{x}(t) = \begin{bmatrix} x_1(t) \\ x_2(t) \\ x_3(t) \end{bmatrix}, \qquad \mathbf{A_o} = \begin{bmatrix} 0 & 1 & 0 \\ -\bar{k}_{11} & -\bar{c}_{11} & 1 \\ 0 & 0 & 0 \end{bmatrix}, \qquad \mathbf{B_o} = \begin{bmatrix} 0 \\ 1 \\ 0 \end{bmatrix},$$

$$\mathbf{E_o} = \begin{bmatrix} 0 \\ \bar{m}_{12} \\ 0 \end{bmatrix}, \qquad \mathbf{F_o} = \begin{bmatrix} 0 \\ 0 \\ 1 \end{bmatrix}, \qquad \mathbf{C_o} = \begin{bmatrix} 1 \\ 0 \\ 0 \end{bmatrix}^{\mathrm{T}},$$

where $x_1(t) = \varphi(t)$, $x_2(t) = \dot{\varphi}(t)$ and $x_3(t) = \xi_\varphi(t)$. Based on this augmented state space system, and the simplified lean angle dynamics of the bicycle (12), the following observer and control law are proposed to govern the output $\varphi(t)$ of the bicycle around zero, independently of the unknown disturbance function $\xi_\varphi(t)$.

Proposition 1 (Disturbance observer for $\xi_\varphi(t)$) *The estimation of the disturbance signal* $\hat{\xi}_\varphi(t)$, *as well as the estimation of each state variable of the simplified system* (12), $\hat{\dot{\varphi}}(t)$ *and* $\hat{\varphi}(t)$, *are obtained by the following observer*:

$$\dot{\hat{\mathbf{x}}}(t) = \mathbf{A_o}\hat{\mathbf{x}}(t) + \mathbf{B_o}u_\varphi(t) + \mathbf{E_o}T_\delta(t) + \mathbf{L_o}\big(\varphi(t) - \hat{\varphi}(t)\big), \tag{18}$$

$$\hat{\varphi}(t) = \mathbf{C_o}\hat{\mathbf{x}}(t), \tag{19}$$

where $\hat{\mathbf{x}}(t) = [\hat{x}_1(t) \;\; \hat{x}_2(t) \;\; \hat{x}_3(t)]^T$ *and* $\mathbf{L_o}$ *is the gain vector of the observer. Then the observer forces the estimation error trajectories* $\tilde{\mathbf{e}}_\mathbf{o}(t) = \mathbf{x}(t) - \hat{\mathbf{x}}(t)$ *to converge towards a small vicinity of zero where remain ultimately bounded, given an appropriate selection of the vector* $\mathbf{L_o}$ *such that the eigenvalues of* $(\mathbf{A_o} - \mathbf{L_o}\mathbf{C_o})$ *are located to the left of the complex plane* s.

Proof See proof in [37]. □

Proposition 2 (Outer-loop control law) *Consider the system* (12) *and assume accurate estimations of* $\hat{\dot{\varphi}}(t)$ *and* $\hat{\xi}_\varphi(t)$, *then the following auxiliary control law*:

$$u_\varphi(t) = -\alpha_1\hat{\dot{\varphi}}(t) - \alpha_0\varphi(t) - \bar{m}_{12}T_\delta(t) - \hat{\xi}_\varphi(t), \tag{20}$$

forces the lean angle of the bicycle to be in a vicinity of zero provided that the gains α_0 *and* α_1 *are selected such that the characteristic polynomial* $s^2 + (\alpha_1 + \bar{c}_{11})s + (\alpha_0 + \bar{k}_{11}) = 0$ *has its roots on the left side of the complex plane* s.

Proof By replacing the auxiliary control law (20) into the open-loop system (12), the expression becomes

$$\ddot{\varphi}(t) + (\alpha_1 + \bar{c}_{11})\dot{\varphi}(t) + (\alpha_0 + \bar{k}_{11})\varphi(t) = \big(\xi_\varphi(t) - \hat{\xi}_\varphi(t)\big) + \alpha_1\big(\dot{\varphi}(t) - \hat{\dot{\varphi}}(t)\big)$$

where, considering accurate estimations of $\hat{\xi}_\varphi(t)$ and $\hat{\dot{\varphi}}(t)$, the estimation errors $(\xi_\varphi(t) - \hat{\xi}_\varphi(t))$ and $(\dot{\varphi}(t) - \hat{\dot{\varphi}}(t))$ of the right side of the equation remain ultimately bounded close to a vicinity of zero; then the dynamic behavior of the lean angle is strongly dominated by the following differential equation:

$$\ddot{\varphi}(t) + (\alpha_1 + \bar{c}_{11})\dot{\varphi}(t) + (\alpha_0 + \bar{k}_{11})\varphi(t) \approx 0. \tag{21}$$

□

Complementary, it is able to observe that increasing the control gain α_0 allows one to reduce the ultimate bound of (21). Thus, the dominant behavior of the lean angle dynamics can be handled as desired.

Remark 2 Note that the auxiliary control law in (20) can be converted into the actual control law of the outer loop, which is in fact the setpoint of the inner control loop δ^*, by manipulating the expression in (13), resulting in:

$$\delta^* = -\frac{1}{\bar{c}_{12}s + \bar{k}_{12}} u_\varphi,$$

where the pole of the system, located at $s = -\bar{k}_{12}/\bar{c}_{12}$, is stable given that the nominal forward speed of the bicycle fulfills the restriction for a minimum-phase zero.

3.1.2 Inner control loop: tracking controller

According to the bicycle dynamics (10), the steering angle dynamics is described by

$$\ddot{\delta}(t) = -\bar{c}_{21}\dot{\varphi}(t) - \bar{c}_{22}\dot{\delta}(t) - \bar{k}_{21}\varphi(t) - \bar{k}_{22}\delta(t) + \bar{m}_{21}T_\varphi(t) + \bar{m}_{22}T_\delta(t), \tag{22}$$

then, lumping together some terms, a simplified version for the steering dynamics is found:

$$\ddot{\delta}(t) = \bar{m}_{22}T_\delta(t) - \bar{c}_{22}\dot{\delta}(t) - \bar{k}_{22}\delta(t) - \bar{c}_{21}\dot{\varphi}(t) - \bar{k}_{21}\varphi(t) + \bar{\xi}_\delta(t), \tag{23}$$

where

$$\bar{\xi}_\delta(t) = \bar{m}_{21}T_\varphi(t). \tag{24}$$

Then, in order to avoid explicit dependency of high order reference trajectories of the steering angle in the control law (i.e. $\dot{\delta}^*(t)$ or $\ddot{\delta}^*(t)$); the system (23) is reformulated in terms of the tracking error of the steering system ($e_\delta(t) = \delta(t) - \delta^*(t)$):

$$\ddot{e}_\delta(t) = \bar{m}_{22}T_\delta(t) - \bar{c}_{22}\dot{e}_\delta(t) - \bar{k}_{22}e_\delta(t) - \bar{c}_{21}\dot{\varphi}(t) - \bar{k}_{21}\varphi(t) + \xi_\delta(t), \tag{25}$$

with

$$\xi_\delta(t) = \bar{\xi}_\delta(t) - \ddot{\delta}^*(t) - \bar{c}_{22}\dot{\delta}^*(t) - \bar{k}_{22}\delta^*(t),$$

where $\xi_\delta(t)$ denotes an additive lumped disturbance function that considers endogenous and exogenous terms of the bicycle system.

Then, given a reference trajectory of the steering angle $\delta^*(t)$, it is desired to force the output $e_\delta(t)$ of the system (25) to zero, regardless of the unknown but uniformly bounded nature of the disturbance function $\xi_\delta(t)$.

Now, to provide estimations of both the states and the disturbance signal $\xi_\delta(t)$ of the system (25), a state space description of the system is required and a local disturbance internal model approximation is assigned into the disturbance signal $\xi_\delta(t)$. In the case of the inner control loop, due to the complexity of the disturbance signal, setting up a low order disturbance internal model approximation would require an observer with high bandwidth, and this will lead to noisy estimations for the inner control loop (for more details see [37, 44]). Therefore, an appropriate selection of the disturbance internal model approximation that provides a good compromise between observer bandwidth and performance of disturbance estimation is defined as

$$\frac{d^4}{dt^4}\xi_\delta(t) \approx 0. \tag{26}$$

Then an augmented system, containing both the states of system (25) and the states of the disturbance model (26), is obtained:

$$\dot{\mathbf{z}}(t) = \mathbf{A_i}\mathbf{z}(t) + \mathbf{B_i}T_\delta(t) + \mathbf{E_{i_1}}\dot{\varphi}(t) + \mathbf{E_{i_2}}\varphi(t) + \mathbf{F_i}\frac{d^4}{dt^4}\xi_\delta(t), \tag{27}$$

$$e_\delta(t) = \mathbf{C_i}\mathbf{z}(t), \tag{28}$$

with

$$\mathbf{z}(t) = \begin{bmatrix} z_1(t) \\ z_2(t) \\ z_3(t) \\ z_4(t) \\ z_5(t) \\ z_6(t) \end{bmatrix}, \quad \mathbf{A_i} = \begin{bmatrix} 0 & 1 & 0 & 0 & 0 & 0 \\ -\bar{k}_{22} & -\bar{c}_{22} & 1 & 0 & 0 & 0 \\ 0 & 0 & 0 & 1 & 0 & 0 \\ 0 & 0 & 0 & 0 & 1 & 0 \\ 0 & 0 & 0 & 0 & 0 & 1 \\ 0 & 0 & 0 & 0 & 0 & 0 \end{bmatrix},$$

$$\mathbf{B_i} = \begin{bmatrix} 0 \\ \bar{m}_{22} \\ 0 \\ 0 \\ 0 \\ 0 \end{bmatrix}, \quad \mathbf{E_{i_1}} = \begin{bmatrix} 0 \\ -\bar{c}_{21} \\ 0 \\ 0 \\ 0 \\ 0 \end{bmatrix},$$

$$\mathbf{E_{i_2}} = \begin{bmatrix} 0 \\ -\bar{k}_{21} \\ 0 \\ 0 \\ 0 \\ 0 \end{bmatrix}, \quad \mathbf{F_i} = \begin{bmatrix} 0 \\ 0 \\ 0 \\ 0 \\ 0 \\ 1 \end{bmatrix}, \quad \mathbf{C_i} = \begin{bmatrix} 1 & 0 & 0 & 0 & 0 & 0 \end{bmatrix},$$

where $z_1(t) = e_\delta(t)$, $z_2(t) = \dot{e}_\delta(t)$, $z_3(t) = \xi_\delta(t)$, $z_4(t) = \dot{\xi}_\delta(t)$, $z_5(t) = \ddot{\xi}_\delta(t)$, and $z_6(t) = \dddot{\xi}_\delta(t)$. Then, based on the augmented system (27) and the reformulated plant (25), the following observer and control law are proposed.

Proposition 3 (Disturbance observer for $\xi_\delta(t)$) *The estimation of the lumped disturbance signal $\hat{\xi}_\delta(t)$, as well as the estimation of $\hat{e}_\delta(t)$ and $\hat{\dot{e}}_\delta(t)$ of the reformulated system* (25), *are obtained by the following observer*:

$$\dot{\hat{\mathbf{z}}}(t) = \mathbf{A_i}\hat{\mathbf{z}}(t) + \mathbf{B_i}T_\delta(t) + \mathbf{E_{i_1}}\dot{\hat{\varphi}}(t) + \mathbf{E_{i_2}}\varphi(t) + \mathbf{L_i}\big(e_\delta(t) - \hat{e}_\delta(t)\big), \tag{29}$$

$$\hat{e}_\delta(t) = \mathbf{C_i}\hat{\mathbf{z}}(t), \tag{30}$$

where $\hat{\mathbf{z}}(t) = [\hat{z}_1(t)\ \ \hat{z}_2(t)\ \ \hat{z}_3(t)\ \ \hat{z}_4(t)\ \ \hat{z}_5(t)\ \ \hat{z}_6(t)]^T$, $\mathbf{L_i}$ *is the gain vector of the observer, and $\dot{\hat{\varphi}}(t)$ is given by the observer in Proposition* 1. *Then the observer* (29)–(30) *forces the estimation error trajectories $\tilde{\mathbf{e}}_\mathbf{i}(t) = \mathbf{z}(t) - \hat{\mathbf{z}}(t)$ to converge towards a small vicinity of zero where it remain ultimately bounded, given an appropriate selection of the vector $\mathbf{L_i}$ such that the eigenvalues of $(\mathbf{A_i} - \mathbf{L_i}\mathbf{C_i})$ are located to the left of the complex plane s.*

Proof See proof in [37]. □

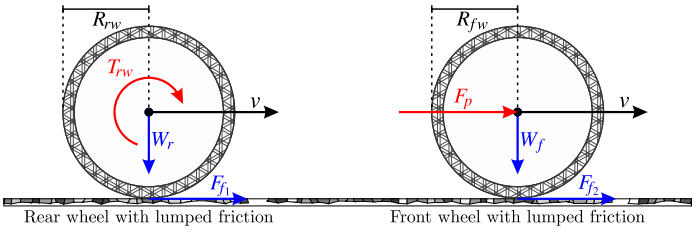

Fig. 7 Free body diagram of rear and front wheels

Proposition 4 (Inner-loop control law) *Consider the system* (25) *and assume accurate estimations of* $\hat{\dot{\varphi}}(t)$, $\hat{e}_\delta(t)$ *and* $\hat{\xi}_\delta(t)$, *then the control law*

$$T_\delta(t) = \frac{1}{\bar{m}_{22}}\left[-\gamma_1 \hat{e}_\delta(t) - \gamma_0 e_\delta(t) + \bar{c}_{21}\hat{\dot{\varphi}}(t) + \bar{k}_{21}\varphi(t) - \hat{\xi}_\delta(t)\right], \tag{31}$$

forces the steering angle of the bicycle $\delta(t)$ *to converge towards a small vicinity of the steering angle reference* $\delta^*(t)$ *as long as the control gains* γ_0 *and* γ_1 *are selected such that the characteristic polynomial,* $s^2 + (\gamma_1 + \bar{c}_{22})s + (\gamma_0 + \bar{k}_{22}) = 0$, *has its roots to the left side of the complex plane* s.

Proof By replacing the control law (31) into the system (25), it results

$$\begin{aligned}\ddot{e}_\delta(t) = &-\bar{c}_{22}\dot{e}_\delta(t) - \gamma_0 e_\delta(t) - \bar{k}_{22}e_\delta(t) - \gamma_1\hat{\dot{e}}_\delta(t) + \bar{c}_{21}\hat{\dot{\varphi}}(t) - \bar{c}_{21}\dot{\varphi}(t)\\ &+ \bar{k}_{21}\varphi(t) - \bar{k}_{21}\varphi(t) + \xi_\delta(t) - \hat{\xi}_\delta(t),\end{aligned}$$

where, after some manipulations, the expression becomes

$$\ddot{e}_\delta(t) + (\gamma_1 + \bar{c}_{22})\dot{e}_\delta(t) + (\gamma_0 + \bar{k}_{22})e_\delta(t) = \tilde{e}_{\xi_\delta}(t) + \gamma_1\tilde{e}_{\dot{e}_\delta}(t) - \bar{c}_{21}\tilde{e}_{\dot{\varphi}}(t),$$

where $\tilde{e}_{\dot{\varphi}}(t) = \dot{\varphi}(t) - \hat{\dot{\varphi}}(t)$, $\tilde{e}_{\xi_\delta}(t) = \xi_\delta(t) - \hat{\xi}_\delta(t)$ and $\tilde{e}_{\dot{e}_\delta}(t) = \dot{e}_\delta(t) - \hat{\dot{e}}_\delta(t)$ are estimation errors. The convergence of $\hat{\dot{\varphi}}(t)$ towards a small vicinity of $\dot{\varphi}(t)$, $\hat{\xi}_\delta(t)$ towards a small vicinity of $\xi_\delta(t)$, and $\hat{\dot{e}}_\delta(t)$ towards a small vicinity of $\dot{e}_\delta(t)$, establishes that the estimation errors, $\tilde{e}_{\dot{\varphi}}(t)$, $\tilde{e}_{\xi_\delta}(t)$ and $\tilde{e}_{\dot{e}_\delta}(t)$, of the right side of the equation, evolve ultimately bounded close to a vicinity of zero. Then the tracking error dynamics of the inner-loop $e_\delta(t) = \delta(t) - \delta^*(t)$ is strongly dominated by

$$\ddot{e}_\delta(t) + (\gamma_1 + \bar{c}_{22})\dot{e}_\delta(t) + (\gamma_0 + \bar{k}_{22})e_\delta(t) \approx 0. \qquad \square$$

3.2 Forward speed controller

Figure 7 shows free-body diagrams for both the rear and the front wheels with forces and momentums lumped at the center of mass when the bicycle is moving in a straight line (with the steering angle close to zero) at a linear, forward speed $v(t)$. W_r and W_f represent the equivalent forces of the bicycle's weight (in N) that act on the wheels' axes ($W_r + W_r = gm_t$), whose relationship between both magnitudes is $\frac{W_f}{W_r} = 0.87$ and defines the prototype's weight distribution—assuming that it is moving on a flat surface—F_{f_1} and F_{f_2} are the exerted friction forces on the wheels by the lower surface, T_{rw} is the applied

torque by the actuator (a DC motor) and F_p is the transmitted pushing force to the front wheel by the bicycle's forward motion.

The bicycle's traction dynamics can be simplified as the set of forces and momentums acting on the wheels to generate its forward motion as Fig. 7 exhibits. Then, considering $v(t) = -R_{rw}\dot{\theta}_r(t)$, which relates the rotation angle of the rear wheel, $\theta_r(t)$, with the forward linear speed, $v(t)$, the following lumped-parameter linear model from Fig. 7 is derived (see [45]):

$$F_{f_1}(t) = -\frac{W_r}{g} R_{rw}\ddot{\theta}_r(t), \tag{32}$$

$$T_{rw}(t) = R_{rw}F_{f_1}(t) - A_{yy}\ddot{\theta}_r(t), \tag{33}$$

$$\mu_{roll} = \frac{F_{f_1}}{F_{n_1}}, \tag{34}$$

where A_{yy} is the wheel's moment of inertia with respect to its spinning axis; $\mu_{roll} = 0.004$ is the assumed rolling friction constant coefficient for both wheels, and F_{n_1} is the normal force on the rear wheel which is proportional to its angular acceleration. Due to the forward motion, the momentum is also present in the front wheel. It is simplified as the set of forces on the front wheel as indicated in Fig. 7. Consequently, the traction dynamics of this wheel is expressed as follows:

$$F_p + F_{f_2} = -\frac{W_f}{g} R_{fw}\ddot{\theta}_f(t), \tag{35}$$

$$\mu_{roll} = \frac{F_{f_2}}{F_{n_2}}, \tag{36}$$

where F_{n_2} is the normal force acting on the front wheel. Pushing force F_p, can be viewed as a perpendicular reaction force on the rear wheel axis, and therefore (35) is added into (32) to find:

$$\underbrace{F_{f_1} + F_{f_2}}_{\text{total friction force}} = -\frac{W_r}{g} R_{rw}\ddot{\theta}_r(t) - \frac{W_f}{g} R_{fw}\ddot{\theta}_f(t), \tag{37}$$

taking into account that $R_{rw} = R_{fw}$ and $\theta_r(t) = \theta_f(t)$. The total friction force and the frictional torque denoted in (4) for the rear wheel joint are then added into (33) to complete the simplified traction model as follows:

$$\begin{aligned} T_{rw}(t) &= R_{rw}\big(F_{f_1}(t) + F_{f_2}(t)\big) - A_{yy}\ddot{\theta}_r(t) - T_f(t), \quad \text{or} \\ T_{rw}(t) &= \left(\frac{A_{yy}}{R_{rw}} + m_t R_{rw}\right)\dot{v}(t) - T_f(t), \end{aligned} \tag{38}$$

given that $\frac{W_r}{g} + \frac{W_f}{g} = m_t$. The model (38) does not consider either slipping nor deformation of the wheels when there is traction. This means that there is no dynamic friction between the wheels and the lower surface, independently of the applied torque (see [46]). Based on the model (38), a PI controller is used to govern the output $v(t)$. Then, by defining $v^*(t)$ as the desired forward speed, the PI control law is expressed as

$$T_{rw}(t) = -K_p e_v(t) - K_i \int_0^t e_v(t)\, dt, \tag{39}$$

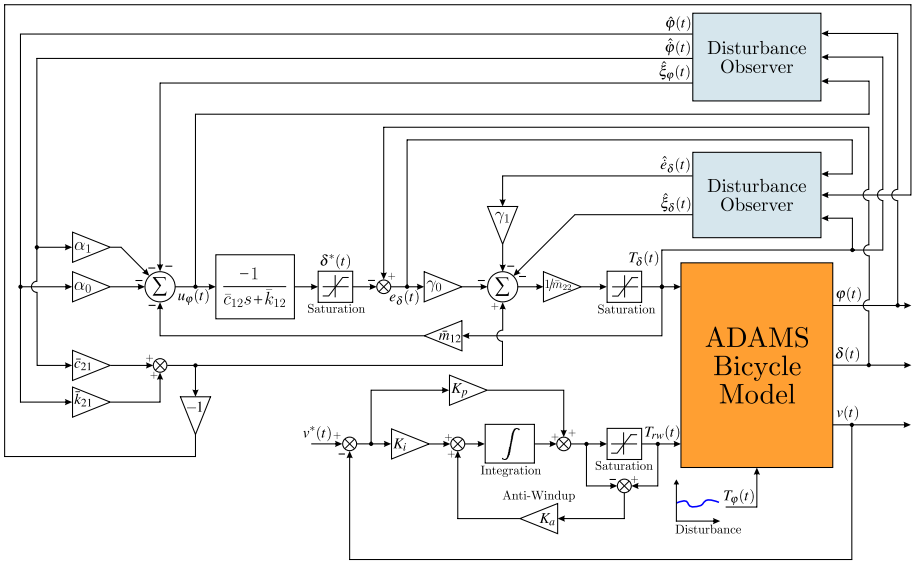

Fig. 8 Detailed blocks diagram of the proposed control strategy

where $e_v(t) = v(t) - v^*(t)$ is the forward speed tracking error. The gains K_p and K_i can be tuned by an arbitrary placement of the poles of the closed-loop system, given by the following characteristic equation:

$$\ddot{e}_v(t) + K_p\dot{e}_v(t) + K_i e_v(t) = \left(\frac{R_{rw}}{A_{yy} + m_t R_{rw}^2}\right)\frac{d}{dt}T_f(t) \approx 0, \tag{40}$$

with

$$K_p = \frac{2(A_{yy} + m_t R_{rw}^2)\zeta\omega_0}{R_{rw}}, \qquad K_i = \frac{(A_{yy} + m_t R_{rw}^2)\omega_0^2}{R_{rw}}, \tag{41}$$

where ζ is the desired relative damping and ω_0 is the desired natural frequency of the closed-loop dynamics.

3.3 Co-simulation of the proposed control strategy

3.3.1 Stabilization and rejection of disturbances

Before implementing the proposed ADRC strategy into the prototype, a co-simulation that uses the built dynamic virtual model in ADAMS/View and the programmed control proposal in MATLAB/Simulink was evaluated. In this co-simulation application, a nominal forward speed of $v_m = 1.5$ m/s is considered, under the proposed control scheme design. This speed is within below the bicycle's self-stabilizing range and above the non-minimal-phase zero zone (see Figs. 3(a) and 3(b)).

For this nominal forward speed, matrices $\bar{\mathbf{M}}$, $\bar{\mathbf{C}}$ and $\bar{\mathbf{K}}$ were calculated. The PI action of forward speed control-loop and the two-stage ADRC loop for stabilizing the lean angle were structured as Fig. 8 shows. This control system was tuned according to the following procedure:

- The forward speed controller was tuned by propounding the closed-loop characteristic polynomial (40) as $(s^2+9.302s+21.633)e_v \approx 0$, where its natural frequency and its relative damping take the values of $\omega_0 = 4.651$ and $\zeta = 1$ respectively. The PI controller gains were calculated by (41) to impose this closed-loop dynamics, obtaining $K_p = 63.654$ and $K_i = 148.032$. This imposed characteristic polynomial allows one to dominate the dynamics of the bicycle forward speed by the poles: $[-4.651 \quad -4.651]$.
- An anti-windup scheme as in [47] was added in the forward speed controller to handle actuator saturation, whose gain was calculated as

$$K_a = 4/(\sqrt{K_i/2K_p}). \tag{42}$$

- The observer in Proposition 1 was designed with $\mathbf{L_o} = [1.557 \times 10^3 \quad 5.386 \times 10^5 \quad 4.148 \times 10^7]^{\mathrm{T}}$, so that the eigenvalues of the estimation error $\tilde{\mathbf{e}}_\mathbf{o}(t)$ were located at $[-1.102 \quad -0.346 \quad -0.109] \times 10^3$ to establish a band-width of (≈ 1000 rad/s) with an adequately damped transient response in the observer.
- The outer-loop control law in Proposition 2 was tuned with $\alpha_0 = 22.412$ and $\alpha_1 = 5.367$, such that the dynamics of the lean angle of the bicycle be dominated by the poles: $[-3.315 \quad -2.419]$.
- The observer in Proposition 3 was tuned with $\mathbf{L_i} = [1.099 \times 10^2 \quad 4.693 \times 10^3 \quad 1.094 \times 10^5 \quad 0.22 \times 10^5 \quad 0.22 \times 10^4]^{\mathrm{T}}$. Then the eigenvalues of the estimation error $\tilde{\mathbf{e}}_\mathbf{i}(t)$ were located at $[-60.065 \quad -26.038+33.566j \quad -26.038-33.566j \quad -0.051+0.088j \quad -0.051-0.088j \quad -0.101]$, which it allowed to establish a band-width of (≈ 97 rad/s) with an adequately damped transient response in this observer.
- The control law of the inner-loop in Proposition 4 was tuned with $\gamma_0 = 448.438$ and $\gamma_1 = 41.538$ which forces the tracking error dynamics $e_\delta(t) = \delta(t) - \delta^*(t)$ to be dominated by the poles: $[-28.633 \quad -15.367]$.

The co-simulation demonstrates that the proposed control strategy effectively stabilizes the virtual prototype from initial condition ($v(0) = 0$ m/s) and with an initial lean angle of $\varphi(0) = 4°$. Figure 9(a) shows the reached forward speed $v(t)$ by the bicycle and the performance of the PI controller in the tracking of reference $v^*(t)$. The applied torque $T_{rw}(t)$ by the PI action to track this reference is shown in Fig. 9(b). Some oscillations appear in the forward speed response due to the applied external force profile on the top of main frame tube with the aim of disturbing the system (see Fig. 9(d)). This external force is applied in the point where [Disturbance_1] indicates in Fig. 4.

Figure 9(c) clearly exhibits that the lean angle controller is effective in the stabilization of $\varphi(t)$, in spite of forward speed variations and the injected external force to the system. The stabilizing controller generates an adequate reference $\delta^*(t)$, which compensates the bicycle instability while the tracking controller imposes a robust tracking of this reference to the steering system, such as in Fig. 9(e). The generated control action by the tracking controller, $T_\delta(t)$, is shown in Fig. 9(f), where the major applied torque is produced when the bicycle is perturbed by the external force to the rear frame, where the predefined saturation limits are exceeded (-10 to 10 Nm).[1]

3.3.2 Stabilization and path tracking

In addition to bicycle stabilization by the proposed robust control strategy, it is also possible to submit the vehicle to the tracking of simple paths on the road flat surface. This path

[1] In the following link: https://youtu.be/7hWhc7an8Ws, the video that shows the interactive co-simulation can be found.

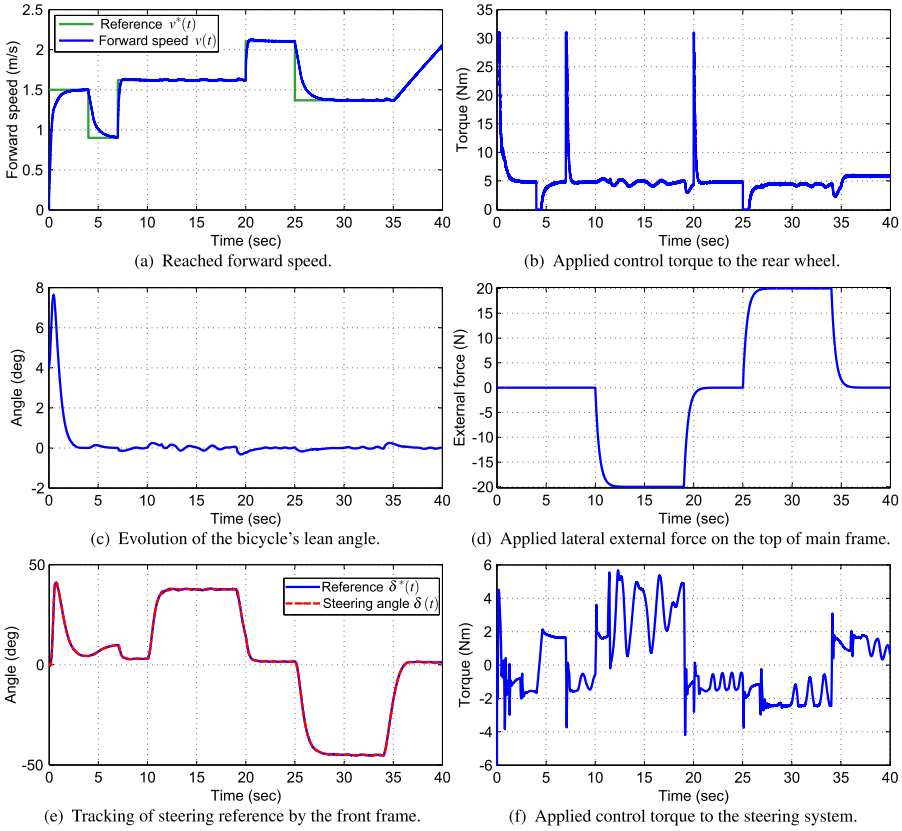

(a) Reached forward speed.
(b) Applied control torque to the rear wheel.
(c) Evolution of the bicycle's lean angle.
(d) Applied lateral external force on the top of main frame.
(e) Tracking of steering reference by the front frame.
(f) Applied control torque to the steering system.

Fig. 9 Results in the co-simulation between MATLAB and ADAMS

tracking can be achieved after the bicycle is totally stable, if it is considered to lead the lean angle to a smooth reference with low rate variations $\varphi^*(t)$. Then the outer control loop of Proposition 2 must be rewritten in terms of the tracking error, $e_\varphi(t) = (\varphi(t) - \varphi^*(t))$, as follows:

$$u_\varphi(t) = -\alpha_1 \dot{e}_\varphi(t) - \alpha_0 e_\varphi(t) - \bar{m}_{12} T_\delta(t) - \hat{\xi}_\varphi(t), \tag{43}$$

where now the associated tracking error dynamics to the lean angle $e_\varphi(t)$ is dominated by the characteristic polynomial $s^2 + (\alpha_1 + \bar{c}_{11})s + (\alpha_0 + \bar{k}_{11}) = 0$, where its roots remain on the left side of the complex plane s.

Subsequent to the bicycle stabilization process at nominal constant forward speed V_m, its multibody dynamics is approximated to the following simple small-perturbation point-mass linear model (see [5]):

$$\ddot{\varphi}(t) = \frac{g}{h}\varphi(t) - \frac{{V_m}^2}{hw}\delta(t) - \frac{bV_m}{hw}\dot{\delta}(t), \tag{44}$$

and the following kinematic equation that relates the lean angle, $\varphi(t)$, with the bicycle orientation angle, $\psi(t)$ (see [48]):

$$\dot{\psi}(t) = \varrho\delta(t) + \vartheta\dot{\delta}(t), \tag{45}$$

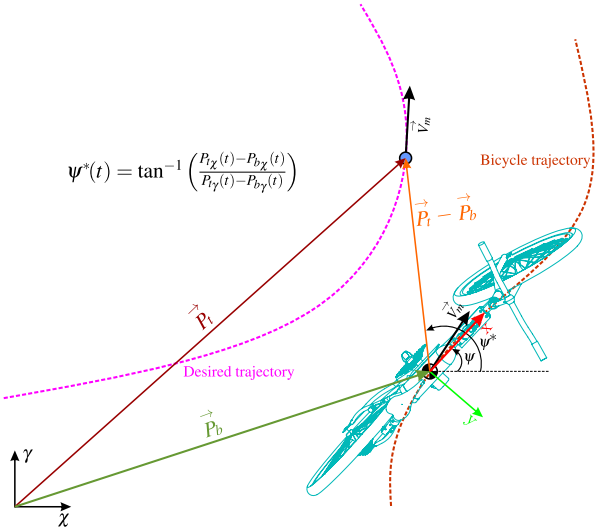

Fig. 10 Schematic approximation of the bicycle kinematics

where its constant coefficients are defined as $\varrho = \frac{V_m}{w}\cos(\frac{\pi}{2} - \eta)$ and $\vartheta = \frac{t_r}{w}\cos(\frac{\pi}{2} - \eta)$. By means of some algebraic manipulation, Eqs. (44) and (45) are combined to obtain the following expression:

$$\frac{\varrho h w}{{V_m}^2}\ddot{\varphi}(t) + \dot{\psi}(t) + \left(\frac{\varrho b}{V_m} - \vartheta\right)\dot{\delta}(t) = \frac{\varrho g w}{{V_m}^2}\varphi(t). \tag{46}$$

Taking into account what the outer control law (43) achieves in its objective ($\varphi(t) = \varphi^*(t)$), it is possible to propound a control strategy to drive the variable $\psi(t)$ from model (46) by the control reference $\varphi^*(t)$. To this purpose, a feedback linearization scheme is formulated, constituted by the following control law:

$$\begin{aligned}\varphi^*(t) = \frac{{V_m}^2}{\varrho g w}\Bigg[&\frac{\varrho h w}{{V_m}^2}\hat{\ddot{\varphi}}(t) + \left(\frac{\varrho b}{V_m} - \vartheta\right)\hat{\dot{\delta}}(t) + \dot{\psi}^*(t) - \beta_1\big(\psi(t) - \psi^*(t)\big) \\ &- \beta_0\int\big(\psi(t) - \psi^*(t)\big)\,dt\Bigg],\end{aligned} \tag{47}$$

which seeks to cancel the associated dynamics to $\ddot{\varphi}(t)$ and $\dot{\delta}(t)$ by their estimations $\hat{\ddot{\varphi}}(t)$ and $\hat{\dot{\delta}}(t)$, them being uniformly and absolutely bounded, and to establish a tracking error dynamics of $e_\psi(t) = (\psi(t) - \psi^*(t))$ dominated by the characteristic polynomial $s^2 + \beta_1 s + \beta_0 = 0$. Polynomial coefficients were selected as $\beta_1 = 0.35$ and $\beta_0 = 0.03$ to force $e_\psi(t)$ to be characterized by the poles $[-0.2 \quad -0.15]$.

Finally, the orientation angle reference $\psi^*(t)$ is obtained from the desired trajectory on the road, such as Fig. 10 shows.

It is assumed that orientation angle, $\psi(t)$, and position vector, $(P_{b_\chi}, P_{b_\gamma})$, of the bicycle are correctly measured when it in motion. $P_t(t)$ is the instantaneous position vector of the desired trajectory from the top view.

The tracking performance of the system for two reference trajectories is presented in Fig. 11. An adequate tracking of a straight line is observed in Fig. 11(a) and the reference $\psi^*(t)$, which drives the bicycle to this path is shown in Fig. 11(b). The additional control

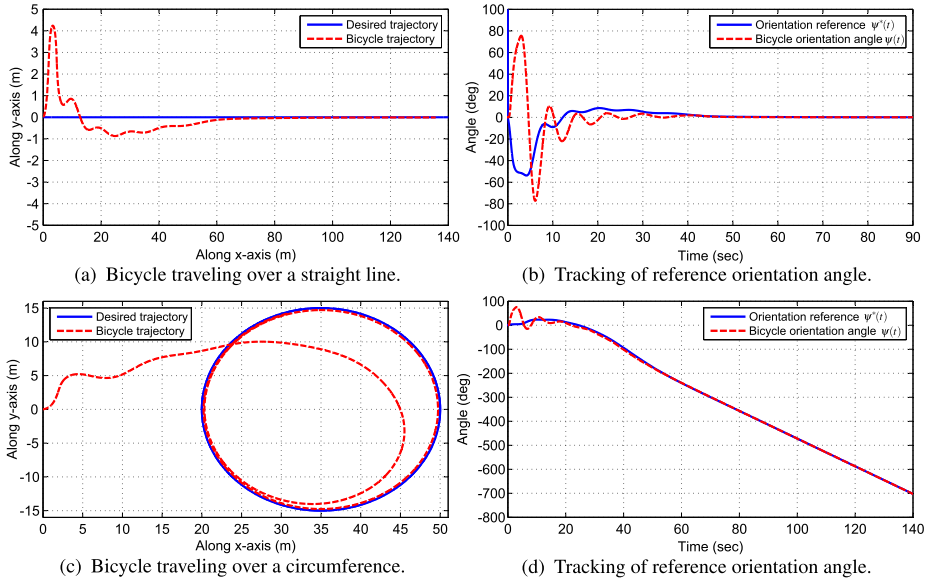

(a) Bicycle traveling over a straight line.
(b) Tracking of reference orientation angle.
(c) Bicycle traveling over a circumference.
(d) Tracking of reference orientation angle.

Fig. 11 Path tracking results in the co-simulation

proposal is also able to impose the tracking of a circumference on the road as Fig. 11(c) shows, which in turn depends on the tracking of the reference $\psi^*(t)$ illustrated in Fig. 11(d).

4 Prototype description

A prototype was built to evaluate the proposed control strategy by using a standard mountain bicycle. The brakes, seat and pedals were removed. For the implementation of the control proposal, the bicycle was equipped with a stand-alone development board, two actuators that provide torque in rear wheel and handlebar axes, three sensors to measure angular speed of rear wheel, lean and steering angles. Finally, two low weight batteries were fixed to the main frame to power all the electrical devices, allowing for a free mobility of the prototype on a runway. A detailed sketch of the distribution of the parts is presented in Fig. 12.

The development board eZdsp™ F28335, made by Spectrum Digital, was selected as the digital processor of the prototype due to its compact dimensions and efficient performance in data processing. For this application, the proposed control scheme was programmed and structured in MATLAB/Simulink®, where information is automatically transferred to CCS (Code Composer Studio)®, which compiles the code to the assembler language and uploads it to the memory of this device, for stand-alone execution with a rate of 150 MHz.

The torque $T_{rw}(t)$ is applied to the rear wheel by means of an industrial DC motor that works at 24 V–3 A, and generates a stall torque of up to 20 Nm. This motor was coupled to the rear wheel axis by the double chain transmission system shown in Fig. 13(a).

The torque $T_\delta(t)$, applied to steering axis, is generated by a Hitec servomotor of reference HS-1000SGT, whose control circuit was removed to directly implement our tracking control proposal on the internal DC motor of this device. This motor is power supplied by a 12.8 V–8 A source, for a stall torque of up to 10 Nm. As depicted in Fig. 13(b), the servomotor

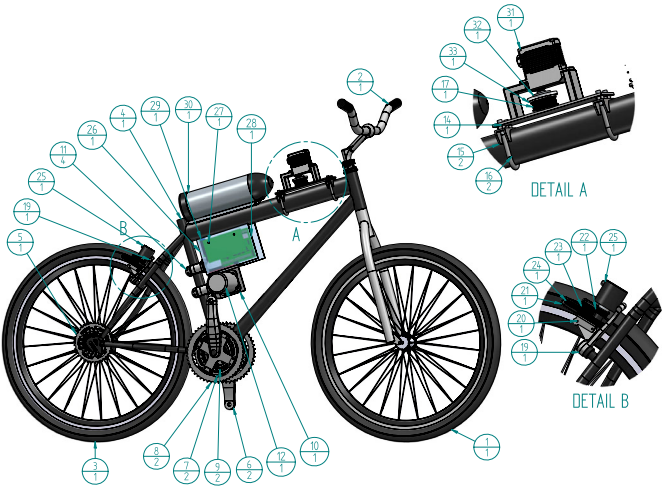

Item	Quantity	Mass (Item)	Comments
1	1	2.051 kg	Front Wheel
2	1	1.950 kg	Handlebar + Front Fork
3	1	2.058 kg	Rear Wheel
4	1	4.850 kg	Rear Frame
5	1	0.550 kg	Cog Set
6	2	0.356 kg	Crank Arm
7	2	0.129 kg	Medium Chainring
8	2	0.141 kg	Large Chainring
9	2	0.074 kg	Small Chainring
10	1	0.470 kg	DC Motor Base
11	4	0.079 kg	Clamps
12	1	1.202 kg	DC Motor
13*	1	0.109 kg	Pinon on DC Motor
14	1	0.313 kg	Servomotor Base
15	2	0.040 kg	Adjusters
16	2	0.056 kg	U-Bolt
17	1	0.057 kg	Pulley
18*	1	0.029 kg	Rear V-Brake (Left Side)
19	1	0.031 kg	Rear V-Brake (Right Side)
20	1	0.013 kg	Backing Piece
21	1	0.056 kg	Pinion Set Housing
22	1	0.014 kg	Encoder Pinion 1
23	1	0.012 kg	Encoder Pinion 2
24	1	0.004 kg	Encoder Pinion 3
25	1	0.198 kg	Encoder
26	1	0.283 kg	Electronic Box
27	1	0.124 kg	eZDSP F28335
28*	1	0.139 kg	Support Card
29	1	0.068 kg	DC-DC Converter
30	1	2.505 kg	Battery
31	1	0.363 kg	Servomotor
32	1	0.008 kg	Horn
33	1	0.011 kg	Acrylic Coupler

Fig. 12 Detailed CAD model of the instrumented bicycle with the weight of each part

(a) Coupling of industrial DC motor with the rear wheel.

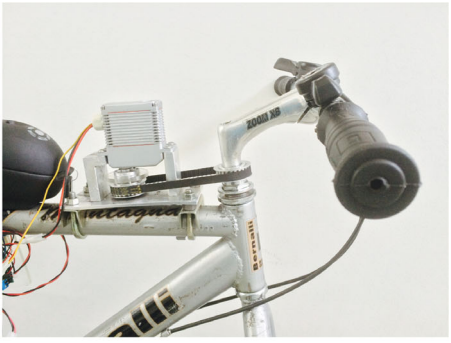

(b) Coupling of Hitec servomotor with the handlebar.

(c) Traction system and assembled sensors to the main frame.

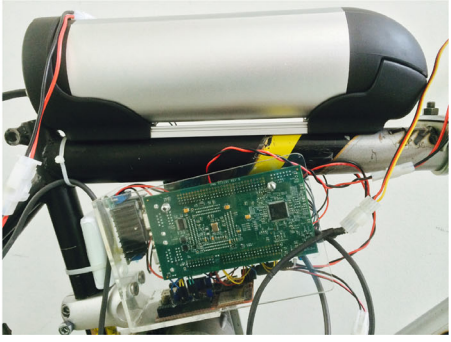

(d) Circuitry box and high power battery.

Fig. 13 Instruments of the robot bicycle prototype

was coupled to the handlebar axis through a transmission system constituted of a toothed belt and two pulleys. Additionally, a high-power H-bridge motor driver, made by Pololu manufacturer, was used in the steering control system.

The control system implementation requires the acquisition in real-time of the forward speed $v(t)$, lean angle $\varphi(t)$ and steering angle $\delta(t)$. The forward speed is measured by means of a YUMO rotary incremental encoder of reference E6B2-CWZ3E, which gives 1024 pulses per revolution. This device was mounted at the right side of the rear wheel, allowing one to compute the bicycle's forward speed using the following operation:

$$v = \frac{1}{T_p}\frac{2\pi r_{pi}}{1024}, \tag{48}$$

where T_p is the encoder quadrature signal period and r_{pi} is the radius of an assembled pinion to the encoder axis that is in constant contact with the rear wheel tire.

The lean angle $\varphi(t)$ is measured by the YEI 3-Space sensor™, which is a miniature, high precision, high-reliability and low cost AHRS (Attitude and Heading Reference System), which uses triaxial gyroscope, accelerometer and compass sensors in conjunction with advanced on-board filtering and processing algorithms to determine orientation relative to an absolute reference orientation in real-time. This sensor was fixed as shown in Fig. 13(c) and configured so that the measured variable be determined by means of Kalman filtering and obtained through its UART communication protocol.

Finally, the steering angle $\delta(t)$ is measured from the built-in servomotor potentiometer, which yields an analog linear output between 0.11 V and 3.2 V for a $\pm 104°$ range.

The eZdsp board and sensors are powered by the small rechargeable 7.4 V lithium ion battery, placed behind the acrylic box such as Fig. 13(c) shows. This battery has a rated capacity of 2.2 Ah, allowing these electronic devices to work for approximately six hours without interruptions. Two actuators are powered by another rechargeable lithium ion battery located above the main frame (see Fig. 13(d)), with an output voltage of 28 V and a rated capacity of 8 Ah. The selection of this battery was due to its low weight in comparison to other acid lead batteries and some accessories that facilitate the mounting onto the bicycle and its charging through the electrical network.

5 Experimental results

5.1 Experimental setup

The complete implementation of the proposed control scheme was performed using the board eZdsp F28335. The board was configured with two high resolution PWMs for driving the actuators of traction and steering systems; one input capture module is used to measure the angular speed of the rear wheel; one UART module is enabled for the communication with the lean angle sensor (YEI 3-space sensor); one analog input is used to read the angular position of the steering system, and an SPI module is configured to store the main variables of the real-time experiment. In Fig. 14, a schematic diagram is shown to explain in detail the overall operation of the control system for the bicycle.

The entire control scheme for controlling the forward speed and stabilizing the lean angle of the bicycle were implemented in the prototype according to the following procedure:

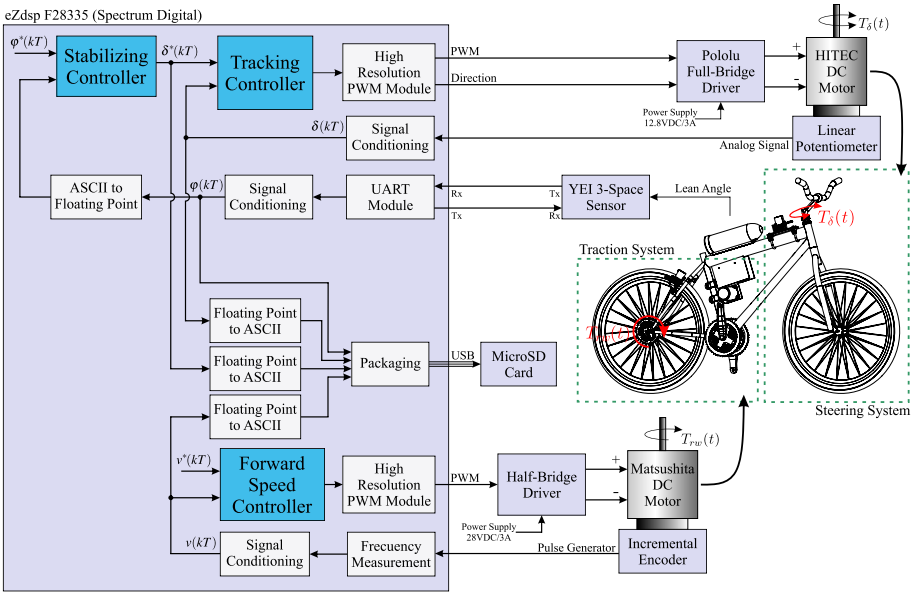

Fig. 14 Implementation block diagram of each control system for the stabilization at constant forward speed in the instrumented bicycle prototype

– The implementation essentially used the same control scheme and tuning of the forward speed controller and lean angle controller described in Sect. 3.3.
– The control input of the steering system $T_\delta(t)$ was converted to a voltage percentage that was applied to a DC motor. The conversion was performed by modifying the control gain ($\bar{m}_{22}$) of (23) to

$$\left(\frac{\bar{m}_{22} K_t K_\epsilon}{R_m}\right), \tag{49}$$

where $K_t = 1.4718$ (rad N m)/A and $R_m = 2.2857\ \Omega$ are the corresponding torque constant and electric resistance of the DC motor, and $K_\epsilon = 12.8/100$ is the gain that relates the PWM percentage in the range of [0–100%] with the actual voltage input applied to the motor. Control input T_δ is determined by the tracking controller and then used in the stabilizing controller according to outer-loop control law in Proposition 2.
– All control scheme was discretized with the Tustin approximation using a sampling time of $T = 0.4$ millis.
– Due to the possible peaking phenomena of the disturbance observers for both $\xi_\delta(t)$ and $\xi_\varphi(t)$, a smoothing discrete function $m(kT)$ ($k = 1, 2, 3, \ldots$, is the discrete variable) was designed to overcome this effect:

$$m(kT) = \begin{cases} \frac{1}{2}(1 - \sin(2\pi kT + \frac{\pi}{2})) & kT < 0.5\text{ s}, \\ 1 & kT \geq 0.5\text{ s}. \end{cases} \tag{50}$$

This function allows for a soft injection of the disturbance estimation into each control law when ($0 < kT < 0.5$ s); then after 0.5 s each disturbance estimation is fully injected (see Fig. 15 for details).

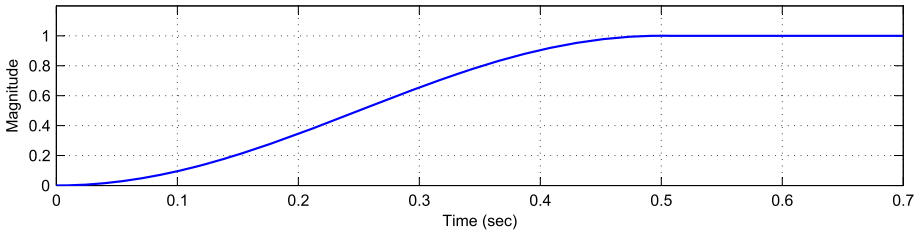

Fig. 15 Smoothing function $m(kT)$ applied to each disturbance estimation of both the stabilizing and the tracking controller

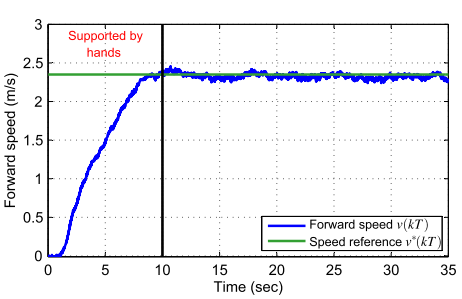

(a) Evolution in time of the bicycle's forward speed with nominal speed of 2.35 m/s.

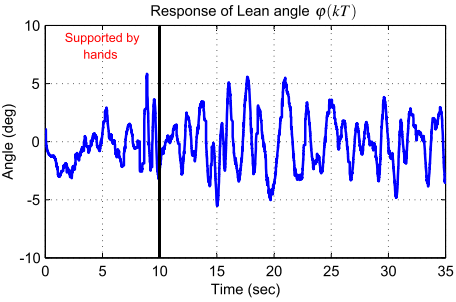

(b) Lean angle around the bicycle's upright position (zero degrees).

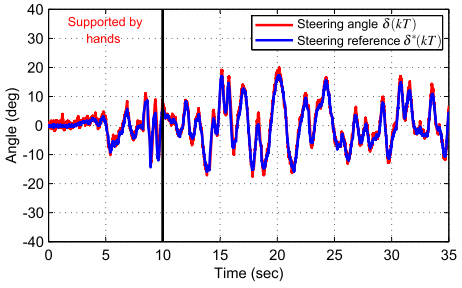

(c) Tracking results of the inner control loop for the steering angle of the bicycle.

(d) Prototype in motion, compensating automatically its instability.

Fig. 16 Closed-loop experimental results of the stabilization of the bicycle prototype obtained during a test using a forward nominal speed of 2.35 m/s

5.2 Experimental results at constant forward speed

The experiment to test the stability of the bicycle with the proposed control scheme was performed on an irregular asphalt street, with an area of 4×80 m^2. In this test, a constant forward speed reference of $v^*(kT) = 2.35$ m/s was used. The evolution in time of the forward speed $v(kT)$ when the prototype is moving on the street is presented in Fig. 16(a). As shown, the bicycle reaches the nominal speed supported and stabilized by hands in around 10 s, then, for a time exceeding 10 s, the proposed two-stage control scheme for stabilizing the bicycle is turned on. The experimental test finishes when the bicycle reaches the space limit given by the size of the street.

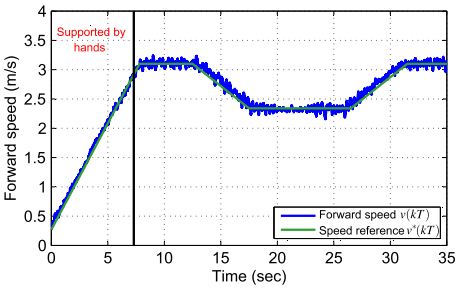

(a) Evolution in time of a bicycle's forward speed profile.

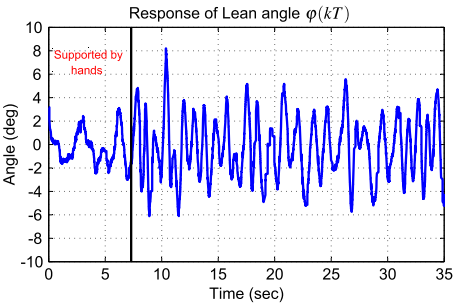

(b) Lean angle response near to the upright position.

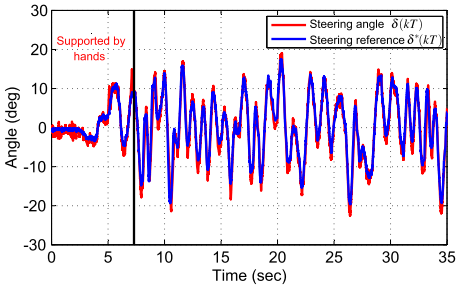

(c) Tracking results of the inner control loop.

(d) Prototype in motion.

Fig. 17 Closed-loop experimental results obtained during a test using a variable forward speed

The lean angle response of the bicycle is shown in Fig. 16(b). This figure illustrates that the bicycle is being stabilized around its upright position by the proposed control scheme and the lean angle $\varphi(kT)$ is changing around zero with minimum/maximum values between ± 5 degrees. This behavior of the lean angle is quite normal due to many disturbances that the bicycle experiments on a real environment, such as crossed winds, irregular street surface, asymmetry of the bicycle, change of the wheels' friction while moving, etc.

Figure 16(c) shows the steering angle reference $\delta^*(kT)$ generated by the stabilizing controller (outer loop) and the response imposed by the tracking controller (inner loop) to the bicycle steering angle $\delta(kT)$. By this illustration, an excellent tracking response for the steering angle developed by the inner control loop can be verified. Figure 16(d) shows a picture of the experimental test of the prototype in motion showing an automatically balanced upright position of the bicycle.[2]

5.3 Experimental results at variable forward speed

Similar to the presented co-simulation results in Sect. 3.3, robustness of the proposed control scheme was also evaluated in an experimental test using a variable forward speed. Thus, a variable forward speed profile was applied as shown in Fig. 17(a). This figure also exhibits the tracking performance of the traction control system.

Despite forward speed variations, the proposed control strategy effectively stabilizes the bicycle. Figure 17(b) shows the response of the lean angle, which is at a steady state bounded

[2]In the following link: https://youtu.be/ks6oLNo0s3o, the video of this experimental test can be found.

within the range of ± 6 degrees. Finally, the steering angle performance can be seen in Fig. 17(c), where a small tracking error is achieved.

6 Concluding remarks

In this paper we have explored, within the context of stabilization problems, the use of approximate yet accurate total active disturbance rejection schemes, based on linear GPI observers for the two stage, outer loop–inner loop, robust controller design stabilization of a riderless bicycle.

The two GPI observer-based control laws recover the performance of the nominal linear model of this plant, establishing a dominant linear dynamics from desired tracking errors. The fundamental advantage of this proposal lies in: an easy linear nominal model-based approach and the single active cancellation of the effects of all unmodeled dynamics, external disturbances and parameter uncertainty associated to the used linear model.

Collaterally, this work presents a novel methodology of linear robust control techniques for arbitrary tracking of reference signals. In particular, the proposed scheme exhibits an enhanced robustness with respect to the variation of zeros of the nominal transfer function due to changes in bicycle's forward speed.

It has been proved that even under the uncertainties of the CAD based model, the proposed control strategy was robust enough to stabilize the lean angle of the instrumented bicycle.

A complete design procedure was presented that covered: Nominal linear plant modeling, ADR controller synthesis, stability analysis, numerical co-simulation and experimental results that showed the feasibility and effectiveness in the solution of the bicycle stabilization problem.

Conflict of interest The authors declare that they have no conflict of interest.

References

1. Herlihy, D.V.: Bicycle: The History, Chap. 1–9. Yale University Press, New Haven (2004)
2. Hamer, M.: Brimstone and bicycles. New Sci. **185**, 44–49 (2005)
3. Sharp, A.: Bicycles and Tricycles: A Classic Treatise on Their Design and Construction, Chap. 14. Dover, New York (2011)
4. Kooijman, J.D.G., Meijaard, J.P., Papadopoulos, J.M., Ruina, A., Schwab, A.L.: A bicycle can be self-stable without gyroscopic or caster effects. Science **332**(6027), 339–342 (2011)
5. Limebeer, D.J.N., Sharp, R.S.: Bicycles, motorcycles, and models. IEEE Control Syst. **26**(5), 34–61 (2006)
6. Åström, K.J., Klein, R.E., Lennartsson, A.: Bicycle dynamics and control: adapted bicycles for education and research. IEEE Control Syst. **25**(4), 26–47 (2005)
7. Schwab, A.L., Meijaard, J.P.: A review on bicycle dynamics and rider control. Veh. Syst. Dyn. **51**(7), 1059–1090 (2013)
8. Meijaard, J.P., Papadopoulos, J.M., Ruina, A., Schwab, A.L.: Linearized dynamics equations for the balance and steer of a bicycle: a benchmark and review. Proc. R. Soc. Lond., Ser. A, Math. Phys. Eng. Sci. **463**(2084), 1955–1982 (2007)
9. Klein, R.E., Lieberman, L., DiRocco, P., McHugh, E.: Adapted bikes deliver new independence: learning to ride a bike is a rite of passage for many children. Except. Parent **32**(10), 64–66 (2002)
10. Klein, R.E., McHugh, E., Harrington, S.L., Davis, T., Lieberman, L.: Adapted bicycles for teaching riding skills. Counc. Except. Child. **37**(6), 50–56 (2005)
11. Chen, C.-K., Dao, T.-K.: A study of bicycle dynamics via system identification. In: International Symposium on Computer, Communication, Control and Automation (3CA), vol. 2, pp. 204–207 (2010)

12. Sharp, R.S.: Optimal stabilization and path-following controls for a bicycle. Proc. Inst. Mech. Eng., Part C, J. Mech. Eng. Sci. **221**(4), 415–427 (2007)
13. Schwab, A.L., Kooijman, J.D.G., Meijaard, J.P.: Some recent developments in bicycle dynamics and control. In: Fourth European Conference on Structural Control (4ECSC), pp. 695–702. Institute of Problems in Mechanical Engineering, Russian Academy of Sciences, Saint-Petersburg (2008)
14. Ai-Buraiki, O., Thabit, M.B.: Model predictive control design approach for autonomous bicycle kinematics stabilization. In: 22nd Mediterranean Conference of Control and Automation (MED), pp. 380–383 (2014)
15. Brizuela, J., Astorga, C., Zavala, A., Pattalochi, L., Canales, F.: State and actuator fault estimation observer design integrated in a riderless bicycle stabilization system. ISA Trans. **61**, 199–210 (2016)
16. Brizuela-Mendoza, J.A., Astorga-Zaragoza, C.M., Zavala-Río, A., Canales-Abarca, F., Reyes-Reyes, J.: Fault tolerant control for polynomial linear parameter varying (LPV) systems applied to the stabilization of a riderless bicycle. In: Control Conference (ECC), 2013 European, pp. 2957–2962 (2013)
17. Varrier, S., Koenig, D., Martinez, J.J.: Integrated fault estimation and fault tolerant control design for LPV systems. IFAC Proc. Vol. **46**(2), 689–694 (2013)
18. Getz, N.: Control of balance for a nonlinear nonholonomic non-minimum phase model of a bicycle. In: American Control Conference, vol. 1, pp. 148–151. Institute of Problems in Mechanical Engineering, Russian Academy of Sciences, Saint-Petersburg (1994)
19. Guo, L., Liao, Q., Wei, S.: Nonlinear stabilization of bicycle robot steering control system. In: International Conference on Mechatronics and Automation, pp. 3185–3189 (2009)
20. Guo, L., Liao, Q.-Z., Wei, S.-M.: Dynamic modeling of bicycle robot and nonlinear control based on feedback linearization of MIMO systems. Beijing Youdian Daxue Xuebao/J. Beijing Univ. Posts Telecommun. **30**(1), 80–84 (2007)
21. Tanaka, Y., Murakami, T.: Self sustaining bicycle robot with steering controller. In: The 8th IEEE International Workshop on Advanced Motion Control, pp. 193–197 (2004)
22. Defoort, M., Murakami, T.: Second order sliding mode control with disturbance observer for bicycle stabilization. In: IEEE/RSJ International Conference on Intelligent Robots and Systems, pp. 2822–2827 (2008)
23. Shafiekhani, A., Mahjoob, M.J., Akraminia, M.: Design and implementation of an adaptive critic-based neuro-fuzzy controller on an unmanned bicycle. Mechatronics **28**(Supplement C), 115–123 (2015)
24. Cerone, V., Andreo, D., Larsson, M., Regruto, D.: Stabilization of a riderless bicycle, a linear-parameter-varying approach [applications of control]. IEEE Control Syst. **30**(5), 23–32 (2010)
25. Gao, Z., Huang, Y., Han, J.: An alternative paradigm for control system design. In: 40th IEEE Conference on Decision and Control, vol. 5, pp. 4578–4585 (2001)
26. Gao, Z.: Active disturbance rejection control: a paradigm shift in feedback control system design. In: Proceedings of the 2006 American Control Conference, 7 pp. (2006)
27. Han, J.: From PID to active disturbance rejection control. IEEE Trans. Ind. Electron. **56**(3), 900–906 (2009)
28. Sira-Ramírez, H., Luviano-Juárez, A., Ramírez-Neria, M., Zurita-Bustamante, E.W.: Active Disturbance Rejection Control of Dynamic Systems: A Flatness Based Approach. Butterworth, Stoneham (2017)
29. Sira-Ramírez, H., Luviano-Juárez, A., Cortés-Romero, J.: Control Lineal Robusto de Sistemas no Lineales Diferencialmente Planos. Rev. Iberoam. Autom. Inform. Ind. RIAI **8**(1), 14–28 (2011)
30. Sira-Ramírez, H., Luviano-Juárez, A., Cortés-Romero, J.: Robust input output sliding mode control of the buck converter. Control Eng. Pract. **21**(5), 671–678 (2013)
31. Ramírez-Neria, M., Sira-Ramírez, H., Garrido-Moctezuma, R., Luviano-Juárez, A.: Linear active disturbance rejection control of underactuated systems: the case of the Furuta pendulum. ISA Trans. **53**(4), 920–928 (2014). Disturbance Estimation and Mitigation
32. Sira-Ramírez, H., Gonzalez-Montanez, F., Cortés-Romero, J.A., Luviano-Juárez, A.: A robust linear field-oriented voltage control for the induction motor: experimental results. IEEE Trans. Ind. Electron. **60**(8), 3025–3033 (2013)
33. Coral-Enriquez, H., Cortés-Romero, J.: Spatial-domain active disturbance rejection control for load mitigation in horizontal-axis wind turbines. In: 2016 IEEE Conference on Control Applications (CCA), pp. 575–580 (2016)
34. Ramírez-Neria, M., Sira-Ramírez, H., Luviano-Juárez, A., Rodríguez-Ángeles, A.: Active disturbance rejection control applied to a delta parallel robot in trajectory tracking tasks. Asian J. Control **17**(2), 636–647 (2015)
35. Ramos, G.A., Cortés-Romero, J., Coral-Enriquez, H.: Spatial observer-based repetitive controller: an active disturbance rejection approach. Control Eng. Pract. **42**(September 2015), 1–11 (2015)
36. Martínez-Fonseca, N., Ángel Castañeda, L., Uranga, A., Luviano-Juárez, A., Chairez, I.: Robust disturbance rejection control of a biped robotic system using high-order extended state observer. ISA Trans. **62**(Supplement C), 276–286 (2016)

37. Cortés Romero, J.A., Ramos, GA., Coral Enriquez, H.: Generalized proportional integral control for periodic signals under active disturbance rejection approach. ISA Trans. **53**(6), 1901–1909 (2014)
38. Cortés Romero, J.A., Luviano Juárez, A., Álvarez Salas, R., Sira Ramírez, H.: Fast identification and control of an uncertain brushless DC motor using algebraic methods. In: 12th International Power Electronics Congress (CIEP), pp. 9–14 (2010)
39. Li, J., Xia, Y., Qi, X., Gao, Z.: On the necessity, scheme, and basis of the linear-nonlinear switching in active disturbance rejection control. IEEE Trans. Ind. Electron. **64**(2), 1425–1435 (2017)
40. Whipple, F.J.W.: The stability of the motion of a bicycle. Q. J. Pure Appl. Math. **30**(120), 312–348 (1899)
41. Papadopoulos, J.M.: Bicycle steering dynamics and self-stability: a summary report on work in progress. Cornell Bicycle Research Project, Cornell University, Ithaca, NY (1987)
42. Pennestrì, E., Rossi, V., Salvini, P., Valentini, P.P.: Review and comparison of dry friction force models. Nonlinear Dyn. **83**(4), 1785–1801 (2016)
43. Baquero-Suárez, M., Cortes-Romero, J., Arcos-Legarda, J., Coral-Enriquez, H.: Estabilización Automática de una Bicicleta sin Conductor mediante el Enfoque de Control por Rechazo Activo de Perturbaciones. Rev. Iberoam. Autom. Inform. Ind. **15**(1), 86–100 (2017)
44. Madoński, R., Herman, P.: Survey on methods of increasing the efficiency of extended state disturbance observers. ISA Trans. **56**(1), 18–27 (2015)
45. Canudas de Wit, C., Tsiotras, P., Velenis, E., Basset, M., Gissinger, G.: Dynamic friction models for road/tire longitudinal interaction. Veh. Syst. Dyn. **39**(3), 189–226 (2003)
46. Canudas de Wit, C., Tsiotras, P.: Dynamic tire friction models for vehicle traction control. In: Proceedings of the 38th IEEE Conference on Decision and Control, vol. 4, pp. 3746–3751 (1999)
47. Åström, K.J., Hägglund, T.: PID Controllers: Theory, Design, and Tuning, Chap. 3, 2nd edn., pp. 80–92. Instrument Society of America (ISA), USA (1995)
48. Schwab, A.L., Meijaard, J.P., Kooijman, J.D.G.: Lateral dynamics of a bicycle with a passive rider model: stability and controllability. Veh. Syst. Dyn. **50**(8), 1209–1224 (2012)